Detection of Surface Resistance in a Gas/Porous-Adsorbent System by Frequency Response Method

Yusuke YASUDA
Faculty of Science, Toyama University, Toyama 930
(Received August 1, 1990)

The frequency-response (FR) method for studying an X⇌C system (Yasuda, 1982) has been extended to an $X \overset{I}{\rightleftharpoons} A \overset{II}{\rightleftharpoons} C$ system, where X denotes a molecule in the gas phase, A is an adspecies on the external surface of a porous adsorbent, and C is an adspecies within micropores. Based on the characteristic functions for a system derived analytically, it is shown that both rate constants for steps I and II can be determined separately from the FR data. According to actual data of CH_4/5A zeolite systems, it has been confirmed that both the adsorption and desorption rate constants for step I, k_a and k_d, respectively, and also the Fickian diffusional time constant at step II, $\widetilde{D}$, can be evaluated. The present method is expected to provide quantitative information conerning the existence and intensity of surface barriers of zeolite crystals.

A frequency-response (FR) method has been applied in order to determine the Fickian diffusivity in zeolite crystals of a pure gas[1] and a binary gas mixture.[2] With zeolites, however, the transport resistance of an adsorbate at the outside of individual crystals occurs due to deposition of an impenetrable material, hydrothermal pretreatment,[3,4] or changes in the crystal structure by a chemical vapor deposition method.[5] Therefore, studying the 'skin' effects seems of interest not only in fundamental research[6] but also regarding industrial applications. Although a micro-dynamic model has recently been proposed for describing the mass-transfer resistance,[7] the six parameters involved in the model seem to be too many to be determined by traditional methods based on time-response data.

The FR method is compared with the standard methods in Table 1, the important characteristic of which is in the volume variation illustrated in Fig. 1; since this method is a resonance-type method, both rate processes during steps I and II could be investigated.

After equilibrium was attained, the gas space of the system V is changed sinusoidally as

$$V(t) = V_e(1 - ve^{i\omega t}), \tag{1}$$

where V_e denotes the equilibrium volume, $v(\ll 1)$ the relative amplitude of the volume change, and ω the angular frequency. The response of the system may be observed in terms of pressure variation, which can generally be expressed by

$$P(t) = P_e\{1 + pe^{i(\omega t + \varphi)}\}, \tag{2}$$

where P_e denotes the equilibrium pressure, p the relative amplitude of the pressure variation, and φ the phase lag between the volume and pressure variation. The dependence of p and φ on ω would reflect the kinetic behavior of the system.

In the present article a theoretical treatment for the system given in Fig. 1 is carried out and some actual data concerning CH_4/5A systems are analyzed in order to confirm the applicability of this new method.

Table 1. Classification of Various Experimental Methods

	Non-equilibrium	Equilibrium
Time-response	Uptake-rate Method Chromatographic Method	NMR Method
Frequency-response		FR Method

Theoretical

Characteristic Functions. The FR of the system may be given by the following in-phase and out-of-phase components, respectively:

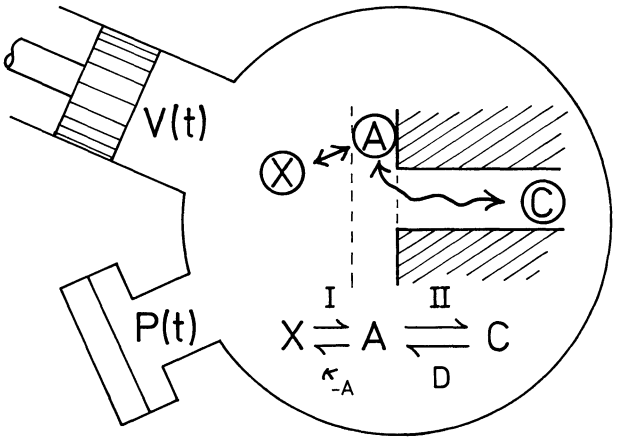

Fig. 1. Schematic diagram of the FR method applied to an X⇄A⇄C system; X denotes the adsorbate in the gas phase, A is the adspecies on the external surface, and C is the adspecies within the porous adsorbent. By measuring the pressure response $P(t)$ to the volume change $V(t)$, the two rate constant κ_{-A} and D at the steps I and II may be determined.

$$(v/p)\cos\varphi - 1 = K \cdot f_c(\omega) \tag{3}$$

and

$$(v/p)\sin\varphi = K \cdot f_s(\omega), \tag{4}$$

where K denotes the asymptote of the in-phase component as $\omega \to 0$. The value of K is expected to agree with K_e given by[1,8]

$$K_e = \left(\frac{RT_0}{V_e}\right)\left\{\frac{d(A+C)}{dP}\right\}_e, \tag{5}$$

where $\{d(A+C)/dP\}_e$ is the gradient of the adsorption isotherm and (RT_0/V_e) is the conversion factor; adspecies on the external surface are denoted by A(and/or B); the adspecies within the porous media are denoted by C.

In the extreme case, where either step I or II is rate-controlling, the present X⇌A⇌C system may be regarded as being an X⇌A or X⇌C system, each of which has been considered previously.[1,8] On the basis of these results, the present complex system can be analytically treated as follows:

(1) In the case of X⇌A, the time course of the A species, $A(t)$, associated with those of $V(t)$ and $P(t)$ in Eqs. 1 and 2 may be described by (Appendix 1)

$$A(t) = A_e[1 + m\{\alpha_c(\kappa_{-A}; \omega) - i\alpha_s(\kappa_{-A}; \omega)\}pe^{i(\omega t + \varphi)}], \tag{6}$$

where

$$m \equiv (d\ln A/d\ln P)_e \tag{7}$$

and A_e denotes the amount of A species at equilibrium.

The FR data of systems f_c and f_s may be expressed in this case by

$$f_c(\omega) = \alpha_c(\kappa_{-A}; \omega) \tag{8}$$

and

$$f_s(\omega) = \alpha_s(\kappa_{-A}; \omega), \tag{9}$$

where the characteristic functions, α_c and α_s, involving one parameter κ_{-A} are given by

$$\alpha_c(\kappa_{-A}; \omega) = \kappa_{-A}^2/(\kappa_{-A}^2 + \omega^2) \tag{10}$$

and

$$\alpha_s(\kappa_{-A}; \omega) = \kappa_{-A}\omega/(\kappa_{-A}^2 + \omega^2). \tag{11}$$

These functions are illustrated in Fig. 2.

2) A more complex system of X⇌A⇌B containing a precursor, A, has also been considered.[8]

The FR data of the system may be described by (Appendix 2)

$$f_c(\omega) = \alpha\alpha_c(\kappa_{-A}, \kappa_{-B}; \omega) \tag{12}$$

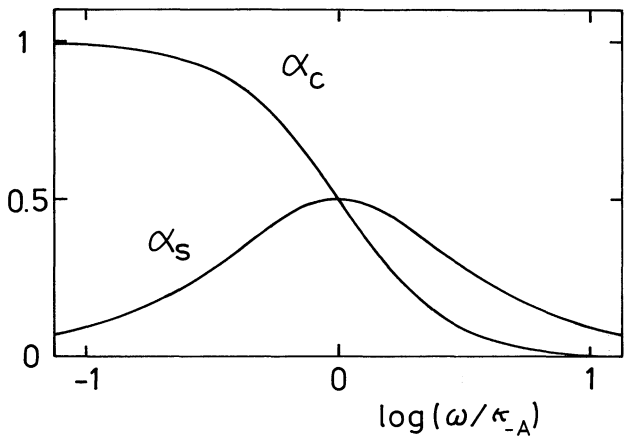

Fig. 2. Characteristic functions for an X⇄A system, $\alpha_c(\kappa_{-A}; \omega)$ and $\alpha_s(\kappa_{-A}; \omega)$; the system corresponds to the extreme case of step I being rate-controlling in Fig. 1.

and

$$f_s(\omega) = \alpha\alpha_s(\kappa_{-A}, \kappa_{-B}; \omega), \tag{13}$$

where the characteristic functions, $\alpha\alpha_c$ and $\alpha\alpha_s$, involving two parameter κ_{-A} and κ_{-B} are given by

$$\alpha\alpha_c(\kappa_{-A}, \kappa_{-B}; \omega) = (a\kappa_{-A}/\omega)^2\{a + b\alpha_c(\kappa_{-B}; \omega)\}/\Phi \tag{14}$$

and

$$\alpha\alpha_s(\kappa_{-A}, \kappa_{-B}; \omega) = (a\kappa_{-A}/\omega)[1 - (a\kappa_{-A}/\omega)\{(a\kappa_{-A}/\omega) + b\alpha_s(\kappa_{-B}; \omega)\}/\Phi]. \tag{15}$$

Here, a short notation is introduced:

$$\Phi \equiv \{(a\kappa_{-A}/\omega) + b\alpha_s(\kappa_{-B}; \omega)\}^2 + \{a + b\alpha_c(\kappa_{-B}; \omega)\}^2. \tag{16}$$

(3) In the case of X⇌C on the other hand, the time course of the C species, $C(t)$, associated with those of $V(t)$ and $P(t)$ in Eqs. 1 and 2 may be described as[1]

$$C(t) = C_e[1 + m'\{\delta_{nc}(\widetilde{D}; \omega) - i\delta_{ns}(\widetilde{D}; \omega)\}pe^{i(\omega t + \varphi)}] \quad (n = 1 \text{ or } 3), \tag{17}$$

where

$$m' \equiv (d\ln C/d\ln P)_e \tag{18}$$

and C_e denotes the amount of C species at equilibrium.

The FR data of the system may be expressed in this case by

$$f_c(\omega) = \delta_{nc}(\widetilde{D}; \omega) \tag{19}$$

and

$$f_s(\omega) = \delta_{ns}(\widetilde{D}; \omega). \tag{20}$$

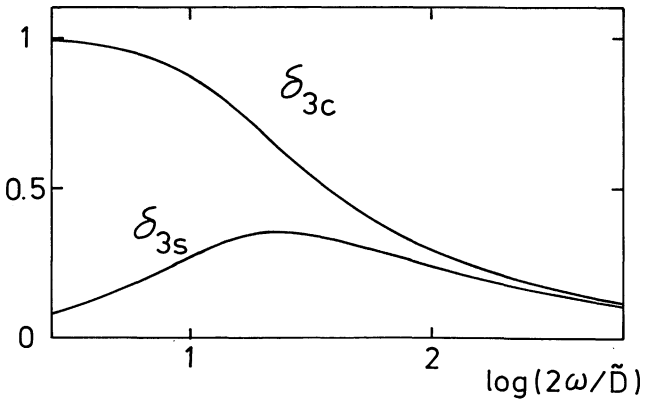

Fig. 3. Characteristic functions for an X⇄C system, $\delta_{3c}(\widetilde{D};\omega)$ and $\delta_{3s}(\widetilde{D};\omega)$; the system corresponds to the extreme case of step II being rate-controlling in Fig. 1.

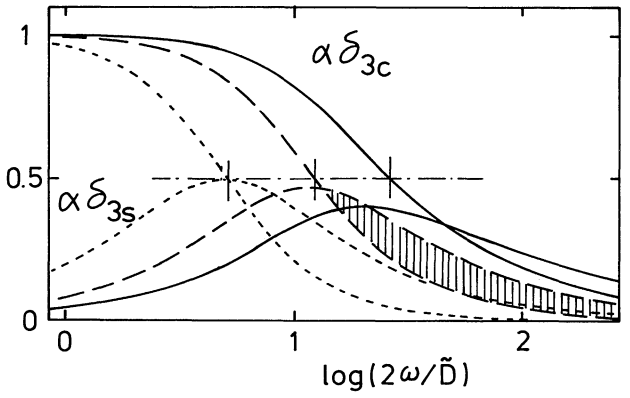

Fig. 4. Characteristic functions for an X⇄A⇄C system, $\alpha\delta_{3c}(\zeta, \widetilde{D};\omega)$ and $\alpha\delta_{3s}(\zeta, \widetilde{D};\omega)$; the parameter ζ is 50 (——), 10 (----), and 3 (·····). It is demonstrated by the shaded area that these curve are intermediate between those in Fig. 2 and in Fig. 3.

The characteristic functions, δ_{nc} and δ_{ns}, involving one parameter, $\widetilde{D}$, are analytically given in Ref. 1; δ_{1c} and δ_{1s} are based on a plane sheet model, and δ_{3c} and δ_{3s} on an isotropic sphere model. The latter functions are applicable to this work with 5A; they are illustrated in Fig. 3.

(4) The FR data of the X⇌A⇌C system are assumed to be expressed by

$$f_c(\omega) = \alpha\delta_{nc}(\kappa_{-A}, \widetilde{D};\omega) \tag{21}$$

and

$$f_s(\omega) = \alpha\delta_{ns}(\kappa_{-A}, \widetilde{D};\omega). \tag{22}$$

The characteristic functions, $\alpha\delta_{nc}$ and $\alpha\delta_{ns}$, involving two parameters, κ_{-A} and $\widetilde{D}$, may be derived from Eqs. 14 and 15 by an analogy between

$$\{\alpha_c, \alpha_s\} \text{ for } X \rightleftharpoons A \rightarrow \{\alpha\alpha_c, \alpha\alpha_s\} \text{ for } X \rightleftharpoons A \rightleftharpoons B$$

and

$$\{\delta_{nc}, \delta_{ns}\} \text{ for } X \rightleftharpoons C \rightarrow \{\alpha\delta_{nc}, \alpha\delta_{ns}\} \text{ for } X \rightleftharpoons A \rightleftharpoons C,$$

since Eq. 17 is similar in form to Eq. 6.

Consequently, we have the final results

$$\alpha\delta_{nc}(\kappa_{-A}, \widetilde{D};\omega) = (a\kappa_{-A}/\omega)^2\{a + c\,\delta_{nc}(\widetilde{D};\omega)\}/\Theta \tag{23}$$

and

$$\alpha\delta_{ns}(\kappa_{-A}, \widetilde{D};\omega) = (a\kappa_{-A}/\omega)[1 - (a\kappa_{-A}/\omega)\{(a\kappa_{-A}/\omega) + c\,\delta_{ns}(\widetilde{D};\omega)\}/\Theta]. \tag{24}$$

Here, a short notation is introduced:

$$\Theta \equiv \{(a\kappa_{-A}/\omega) + c\delta_{ns}(\widetilde{D};\omega)\}^2 + \{a + c\,\delta_{nc}(\widetilde{D};\omega)\}^2 \tag{25}$$

and

$$c \equiv (dC/dP)_e/\{d(A + C)/dP\}_e \equiv 1 - a. \tag{26}$$

Three typical curves of $\alpha\delta_{3c}$ and $a\delta_{3s}$ for different choices of the values for $a\kappa_{-A}$ and $\widetilde{D}$ are compared in Fig. 4, where $a \ll 1$; that $c \fallingdotseq 1$ are assumed, because they are usually satisfied with zeolites (as discussed below). The shaded area demonstrates that these functions are intermediate in shape between the curves given in Fig. 2 and those in Fig. 3. It is worth noting that the shaded area, or the peak height of $\alpha\delta_{3s}$ depends on the ratio of ζ, defined by

$$\zeta \equiv a\kappa_{-A}/\widetilde{D}. \tag{27}$$

The Fickian diffusional time constant, $\widetilde{D}$, is given in the case of the isotropic sphere model by[1)]

$$\widetilde{D} = D/r_m^2, \tag{28}$$

where D is the Fickian diffusivity and r_m is the radius of the sphere. On the other hand, the fraction, a, is expected to be approximately proportional to r_m^{-1}, since the ratio of the external surface area to the volume of the sphere is $3/r_m$. We, thus, have

$$\zeta \propto (\kappa_{-A}/D)r_m, \tag{29}$$

suggesting that 'skin' effects depend not only on the ratio of the rate constants at steps I and II, κ_{-A}/D, but also on the size of the crystals, which is in accordance with experimental findings.[3a)]

Crystal-Size Distribution. The microcrystal sizes of synthetic zeolites are usually not identical, but distributed. The distribution may be regarded as being almost normal.[9)] In a data analysis, therefore, δ_{nc} and δ_{ns} in Eqs. 23 and 24 should be modified as

$$\bar{\delta}_{nj}\left(\frac{D}{r_m{}^2};\omega\right)=\frac{1}{(2\pi)^{\frac{1}{2}}\sigma}\int_0^\infty \delta_{nj}\left(\frac{D}{r^2};\omega\right)\exp\left\{-\frac{(r-r_m)^2}{2\sigma^2}\right\}dr \quad (j=\text{c or s}), \tag{30}$$

where σ is the standard deviation and r_m is the mean radius, provided that $n=3$.

Evidently, when the crystal-size distribution is considered, Eqs. 21 and 22 should be modified as

$$f_c(\omega)=\alpha\bar{\delta}_{nc}(\zeta,\widetilde{D};\omega) \tag{31}$$

and

$$f_s(\omega)=\alpha\bar{\delta}_{ns}(\zeta,\widetilde{D};\omega), \tag{32}$$

where

$$\alpha\bar{\delta}_{nc}(\zeta,\widetilde{D};\omega)=(a\kappa_{-A}/\omega)^2\{a+c\,\bar{\delta}_{nc}(\widetilde{D};\omega)\}/\bar{\Theta} \tag{33}$$

and

$$\alpha\bar{\delta}_{ns}(\zeta,\widetilde{D};\omega)=(a\kappa_{-A}/\omega)[1-(a\kappa_{-A}/\omega)\{(a\kappa_{-A}/\omega)+c\,\bar{\delta}_{ns}(\widetilde{D};\omega)\}/\bar{\Theta}]. \tag{34}$$

Here, a short notation is introduced:

$$\bar{\Theta}\equiv\{(a\kappa_{-A}/\omega)+c\bar{\delta}_{ns}(\widetilde{D};\omega)\}^2+\{a+c\,\bar{\delta}_{nc}(\widetilde{D};\omega)\}^2. \tag{35}$$

Equations 31—35, after substitution of $n=3$ and $c=1$, were applied to a data analysis of CH_4/5A systems in this work.

It is worth noting that if the kinetic behavior at step I is described by a *Langmuir-type* rate equation, κ_{-A} may be given by[8]

$$\kappa_{-A}=k_aP_e+k_d, \tag{36}$$

where k_a and k_d denote the adsorption and desorption rate constants, respectively.

Experimental

Materials. A synthetic zeolite (5A) was supplied by Tosoh Corporation (A-30; designated as Linde 5A); its properties are summarized in Table 2. For a comparison, Linde 5A supplied commercially was used after the preparation described previously.[10]

Methane in a commercial cylinder (99.99% pure; data in catalogue) was used without any further purification.

Table 2. Properties of A-30

Cation exchange	$CaO/(CaO+Na_2O)=0.70$
Mean edge length	3.0 μm
Pretreatment	(i) pelleted with binder, (ii) calcined at 400—500 °C for 1—2 h, (iii) moistened with water, and (iv) calcined again.

Apparatus and Procedure. Both the FR apparatus and procedure were similar to those described previously;[1,11] blank experiments were carried out with He under almost the same conditions as those with CH_4.

Results and Discussion

(1) A-30 Systems. Changes in the FR data at different equilibrium temperatures (T_e) are shown in Figs. 5—8; these data were divided by the value of K_F given in Table 3. The value of K_e evaluated from the adsorption isotherm according to Eq. 5 is also given in Table 3. The agreement between K_F and K_e suggests that all FR data of the system were detected in the ω-region scanned.

All solid curves represent the calculated results from Eqs. 33 and 34, where the value of σ/r_m concerned with the crystal-size distribution was assumed to be 0.4.[9b] Two parameters, ζ and $\widetilde{D}$, were determined on a trial-and-error basis from the shape of f_c and f_s; the value of ζ was easily estimated from the area corresponding to

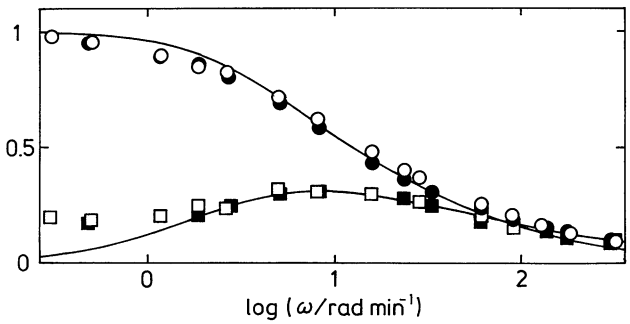

Fig. 5. FR data of CH_4/A-30 systems at −78 °C; the in-phase and the out-of-phase components, f_c and f_s, are represented by the circles and the squares, respectively; each component was divided by K_F given in Table 3. ● and ■ represent the data obtained under P_e=2.7 Torr; ○ and □, those under P_e=4.5 Torr. The solid curve are calculated from Eqs. 33 and 34 of which parameters, ζ and $\widetilde{D}$, are given in Table 3.

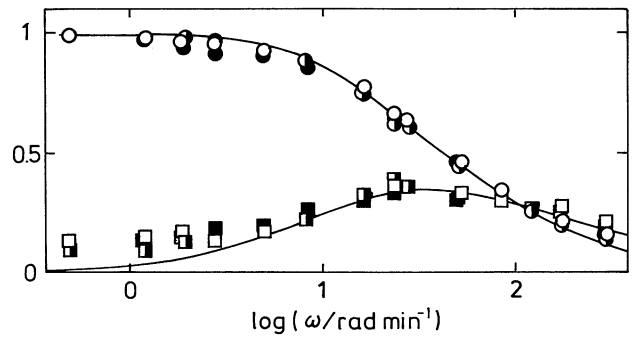

Fig. 6. FR data of CH_4/A-30 systems at T_e=−50 °C. ● and ■ represent the data under P_e=3.0 Torr; ◑ and ◨, those under P_e=5.8 Torr; ○ and □, those under P_e=7.3 Torr. Notation is that of Fig. 5.

the shaded area in Fig. 4. The results are summarized in Table 3; the shift of the peak maximum of f_s has revealed an increase of $\widetilde{D}$ with increasing T_e, while an increase in the overlapping area leads to a decrease in ζ.

The deviation of f_s from the theoretical curves in the lower ω-region in Fig. 5 decreased with increasing T_e; the disagreement of K_F with K_e also decreased. This fact suggests that although the model in Fig. 1 is valid at higher T_e, the contribution of another immobile adspecies besides A and C increased with the decreasing T_e.

Arrhenius plots of the values of $a\kappa_{-A}$ ($=\zeta\widetilde{D}$; Eq. 27) and $\widetilde{D}$ are shown in Fig. 9; the activation energy of the intracrystalline diffusion, E_D, evaluated from the solid straight line was 19.1 kJ mol^{-1}, which was comparable with the heat of adsorption, ($-\Delta H=$) 19.8 kJ mol^{-1}, calculated from K_e's at $T_e=-50$ and -21 °C in Table 3 according to Clausius–Clapeyron equation.

The dependence of f_c and f_s on P_e was so slight (Fig. 8) that it was difficult to directly evaluate k_a and k_d from Eq. 36. However, on the basis of the shift indicated by the light lines in Fig. 8, we can estimate the values of k_a and k_d as follows:

(i) $\omega_{\frac{1}{2}}$ is introduced by

$$\alpha\bar{\delta}_{3c}(\zeta, \widetilde{D}; \omega_{\frac{1}{2}}) = \frac{1}{2} \tag{37}$$

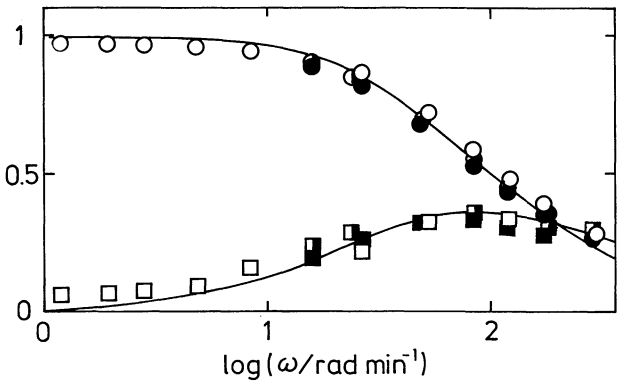

Fig. 7. FR data of CH_4/A-30 systems at $T_e=-21$ °C. ● and ■ represent the data under $P_e=3.0$ Torr; ◑ and ◨, those under $P_e=4.3$ Torr; ○ and □, those under $P_e=6.7$ Torr. Notation is that of Fig. 5.

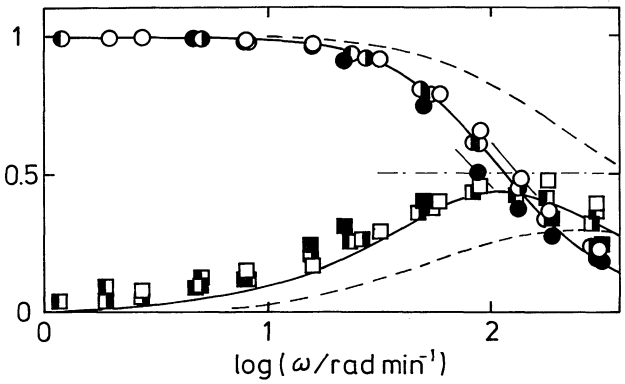

Fig. 8. FR data of CH_4/A-30 systems at $T_e=0$ °C. ● and ■ represent the data under $P_e=1.6$ Torr; ◑ and ◨, those under $P_e=3.0$ Torr; ◐ and ◧, those under $P_e=3.4$ Torr; ○ and □, those under $P_e=4.8$ Torr. Notation is that of Fig. 5. The additional dotted curves of Eq. 30 represent the extreme case of $\zeta\to\infty$; the difference between the two kinds of curves demonstrates, therefore, the transport resistance at step I.

Table 3. Experimental Conditions and Rate Constants Derived

Zeolite	m[a]	T_e	P_e	K_e	K_F	ζ	$\widetilde{D}$	$a\kappa_{-A}$[c]$\times10^{-3}$	$ak_a\times10^{-2}$	$ak_d\times10^{-2}$
	g	°C	Torr[b]				min^{-1}	min^{-1}	Torr^{-1} min^{-1}	min^{-1}
A-30	13.75	−78	2.7	—	11.4	2×10²	0.63	0.13	—	—
			4.5	—	8.4					
	25.82	−50	3.0	7.5	4.9					
			5.8	7.5	4.6	6×10	2.7	0.17	—	—
			7.3	7.5	4.5					
	25.82	−21	3.0	2.2	2.1					
			4.3	2.2	2.0	4×10	7.5	0.30	—	—
			6.7	2.2	1.7					
	101.74	0	1.6	4.2	4.8			0.15		
			3.0	4.2	6.0	10	18.8	0.19	0.3	1.0
			3.4	4.2	4.8					
			4.8	4.2	4.4			0.24		
Linde-5A	24.30	0	3.4	0.73	0.60	4×10		0.28		
			4.4	0.73	0.67	6×10	7.1	0.43	1.2	ca. 0
			9.0	0.73	0.90	2×10²		1.42		

a) The weight of the adsorbent in a dehydrated state. b) 1 Torr=133.3 Pa. c) $a\fallingdotseq6\times10^{-3}$.

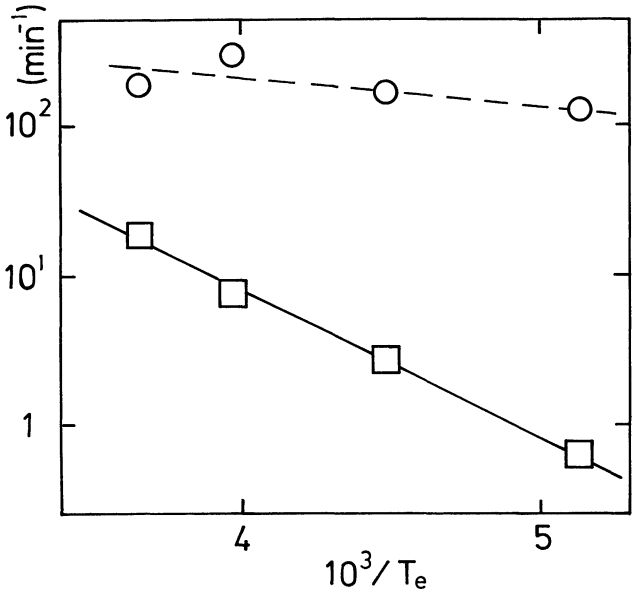

Fig. 9. Arrhenius plots of the parameters, a κ_{-A} (○) and $\widetilde{D}$ (□), derived from the solid theoretical curves shown in Figs. 5—8.

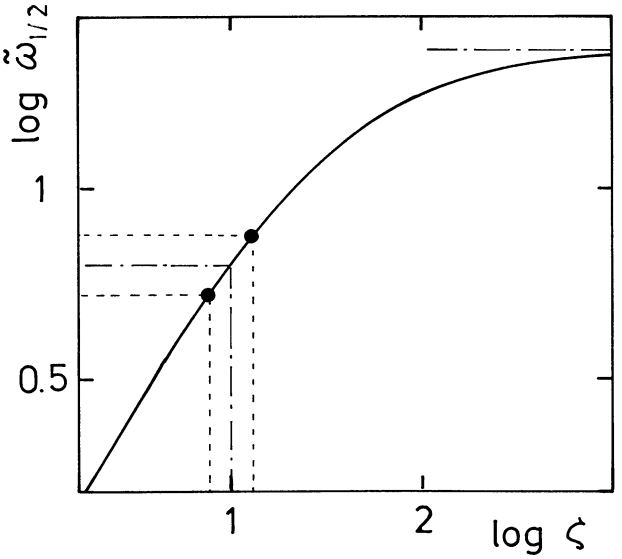

Fig. 10. The center position of the theoretical curve $\alpha\delta_{3c}(\zeta, \widetilde{D}; \omega)$ represented by $\widetilde{\omega}_{1/2}$ versus ζ; the shifts are demonstrated by the vertical lines in Fig. 4. The asymptote indicated on the right is 1.363.

and $\widetilde{\omega}_{\frac{1}{2}}$ is defined by

$$\widetilde{\omega}_{\frac{1}{2}} = \omega_{\frac{1}{2}}/\widetilde{D}. \tag{38}$$

(ii) $\widetilde{\omega}_{\frac{1}{2}}$ depends on ζ, as demonstrated by the vertical lines in Fig. 4. The extended dependence is illustrated in Fig. 10.

(iii) The shift of $\log \omega_{\frac{1}{2}}$ in Fig. 8, indicated by the two light lines, was 0.17.

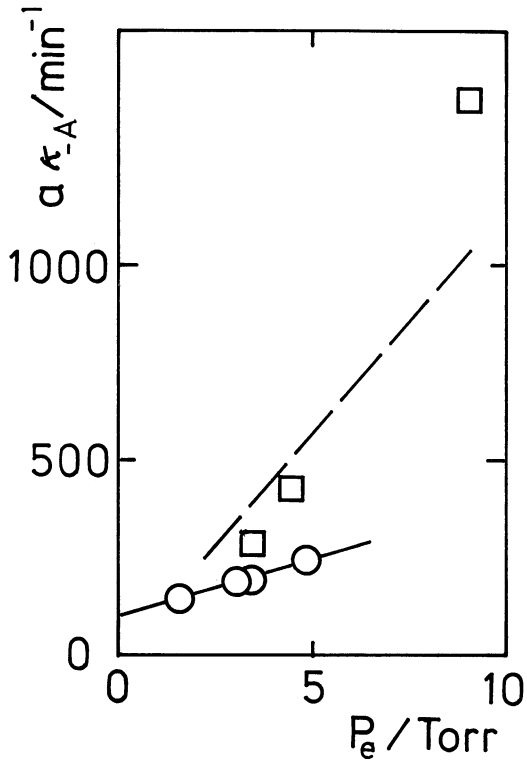

Fig. 11. Rate constant at step I, a κ_{-A}, versus P_e. ○'s represent the results of A-30; □'s, those of Linde 5A. The straight lines lead to the values of ak_a and ak_d given in Table 3.

(iv) The mean value of ζ was 10 (see Table 3).

(v) A shift by 0.17 of $\Delta\log \omega_{\frac{1}{2}}(=\Delta\log \widetilde{\omega}_{\frac{1}{2}})$ leads to 0.22 for $\Delta\log \zeta$, indicated by the solid circles in Fig. 10.

(vi) Consequently, we have (1 Torr=133.322 Pa)

$$\zeta = \begin{cases} 13 & \text{at } P_e = 4.8 \text{ Torr} \\ 7.8 & \text{at } P_e = 1.6 \text{ Torr.} \end{cases} \tag{39}$$

(vii) The values of $a\kappa_{-A}(P_e)$ evaluated from $\zeta(P_e)\times\widetilde{D}$ are plotted in Fig. 11; since the adsorption isotherm at T_e=0 °C was proportional to P_e, $\widetilde{D}$ was assumed to be independent of P_e.[12]

(viii) Under the assumption of Eq. 36, we found the values of ak_a and ak_d from the straight line in Fig. 11; they are given in Table 3.

(2) Linde 5A Systems. In order to determine the effects of a hydrothermal pretreatment of A-30, additional experiments were carried out. The FR data of Linde 5A (without the hydrothermal pretreatment) are shown in Fig. 12.

The dashed and the solid curves were calculated from Eqs. 33 and 34 under the assumption that σ/r_m=0.5.[10] In this case, the pressure dependence of $\zeta(P_e)$ was determined directly by curve fittings under the assumption of constant $\widetilde{D}$; these results are given in Table 3.

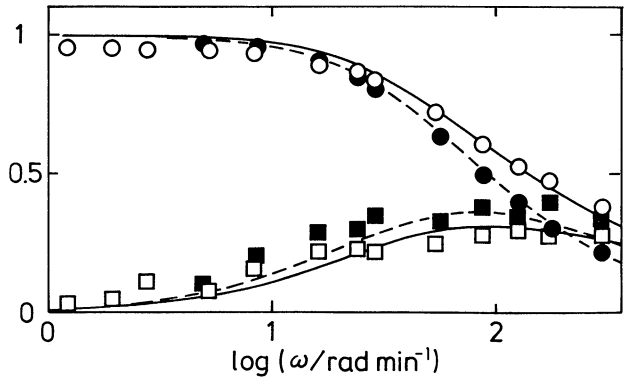

Fig. 12. FR data of CH_4/Linde 5A systems at T_e= 0°C. ● and ■ represent the data under P_e=3.4 Torr; ○ and □, those under P_e=9.0 Torr. The dashed and the solid curves are calculated from Eqs. 33 and 34, of which parameters are given in Table 3.

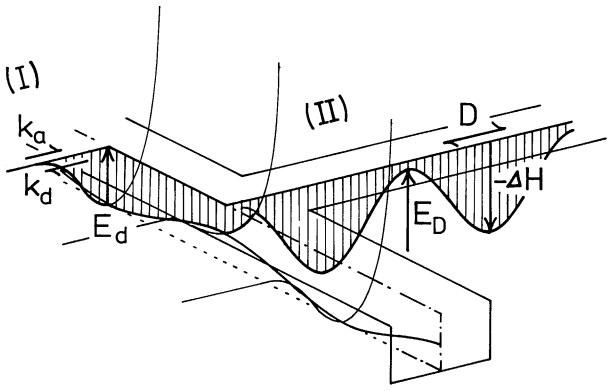

Fig. 13. The potential energy distribution of the X⇄A⇄C system in Fig. 1. Every six constant characteristic of the adsorbate-adsorbent system may be evaluated from the FR data analysis: k_a and k_d denote adsorption and desorption rate constants, respectively; E_d is the activation energy of the desorption; D is the Fickian diffusivity; E_D is the activation energy of the diffusion; $-\Delta H$ corresponds to the heat of adsorption.

The values of $a\kappa_{-A}(P_e)$ evaluated from ζ and $\widetilde{D}$ are plotted in Fig. 11. Though the results seem to be scattered, it may be concluded that the value of k_a is considerably larger than that of A-30, whereas k_d is very smaller than that of A-30; it is worth noting that Eq. 36 is valid only if the Langmuir-type equation is accepted.

The value of a is expected to be about 6×10^{-3}, since the external BET surface area of 5A zeolites was 0.6% of the entire surface area.[13] The absolute value of k_d is, therefore,

$$k_d = 1.7 \times 10^4 \text{ min}^{-1} \text{ for A-30.} \quad (40)$$

The mean lifetime of A-species, τ_A, can be given by the inverse of k_d,

$$\tau_A = 4 \times 10^{-3} \text{ s.}$$

Since k_d of the Linde 5A system was considerably smaller than that of A-30, a hydrothermal pretreatment made the lifetime of the A-species considerably shorter.

(3) Effect of Intercrystalline Diffusion. The theoretical curves based on the model in Fig. 1 without intercrystalline diffusion were valid for explaining all of the FR data given in Figs. 5—8 and Fig. 12. Therefore, the resistance due to intercrystalline diffusion may be neglected. The large difference of ak_a or ak_d in Table 3 with respect to the different adsorbents also supports this conclusion, since A-30 is designated as Linde 5A.

Conclusion

According to the theoretical procedure proposed in this work, the potential energy distribution illustrated in Fig. 13 may be derived from FR data, though we have no information about surface diffusion along the external surface. It is worth noting that all six constants do not depend on the amount of adsorbent but, rather, on the structure. Therefore, the present method would provide quantitative information concerning the existence and intensity of surface barriers of zeolite crystals.

Appendix 1

The variation of the A-species may be expressed as

$$A(t) = A_e\{1 + ae^{i(\omega t + \varphi - \psi)}\}. \quad (A1)$$

According to the result in Eq. 19 of Ref. 8, we find

$$a = mp\kappa_{-A}/(\kappa_{-A}^2 + \omega^2)^{\frac{1}{2}}. \quad (A2)$$

On the other hand, we have the result

$$\tan\psi = \omega/\kappa_{-A}. \quad (A3)$$

Substitution of Eqs. A2 and A3 into Eq. A1 leads to Eq. 6.

Appendix 2

The FR of an X⇌A⇌B system has been considered[8] and the results are rewritten in terms of α_c and α_s defined by Eqs. 10 and 11:

$$(v/p)\cos\varphi - 1 = K_A(\kappa_{-A}^2/\omega^2)\{1 + K_B\alpha_c(\kappa_{-B};\omega)\}/\Phi' \quad (A4)$$

and

$$(v/p)\sin\varphi = K_A(\kappa_{-A}/\omega)[1 - (\kappa_{-A}/\omega)\{(\kappa_{-A}/\omega) + K_B\alpha_s(\kappa_{-B};\omega)\}/\Phi'], \quad (A5)$$

where the relation of $\kappa_q/\kappa_{-q}=K_q$ in Eq. 18 of Ref. 8 is considered and a short notation is introduced:

$$\Phi' \equiv \{(\kappa_{-A}/\omega) + K_B\alpha_s(\kappa_{-B};\omega)\}^2 + \{1 + K_B\alpha_c(\kappa_{-B};\omega)\}^2. \quad \text{(A6)}$$

Considering the asymptote as $\omega\to 0$ in Eq. A4, we have

$$\lim_{\omega\to 0}(v/p)\cos\varphi - 1 = K_A(1 + K_B). \quad \text{(A7)}$$

On the other hand, the asymptote may be correlated with the gradient of the adsorption isotherm:[8]

$$\lim_{\omega\to 0}(v/p)\cos\varphi - 1 = (RT_0/V_c)\{d(A + B)/dP\}_c \ (\equiv K_c'). \quad \text{(A8)}$$

A comparison of Eq. A7 with Eq. A8 leads to

$$K_A = aK_c' \quad \text{and} \quad K_B = b/a, \quad \text{(A9)}$$

where a short notation is introduced:

$$a \equiv (dA/dP)_c/\{d(A + B)/dP\}_c \equiv 1 - b. \quad \text{(A10)}$$

Substitution of the relation in Eq. A9 into Eqs. A4 and A5 leads to the final results of Eqs. 12—16.

References

1) Y. Yasuda, *J. Phys. Chem.*, **86**, 1913 (1982).

2) Y. Yasuda and K. Matsumoto, *J. Phys. Chem.*, **93**, 3195 (1989).

3) a) M. Bülow, P. Struve, G. Finger, C. Redszus, K. Ehrhardt, and W. Schirmer, *J. Chem. Soc., Faraday Trans. 1*, **76**, 597 (1980), b) M. Bülow, P. Struve, and S. Pikus, *Zeolites*, **2**, 267 (1982).

4) a) J. Kärger, W. Heink, H. Pfeifer, and M. Rauscher, *Zeolites*, **2**, 275 (1982), b) J. Kärger and H. Pfeifer, *Zeolites*, **7**, 90 (1987).

5) M. Niwa, M. Kato, T. Hattori, and Y. Murakami, *J. Phys. Chem.*, **90**, 6233 (1986).

6) J. Crank, "The Mathematics of Diffusion," Clarendon Press, Oxford (1964), p. 195.

7) M. Kocirik, P. Struve, K. Fiedler, and M. Bülow, *J. Chem. Soc., Faraday Trans. 1*, **84**, 3001 (1988).

8) Y. Yasuda, *J. Phys. Chem.*, **80**, 1867 (1976).

9) a) K. F. Loughlin, R. I. Derrah, and D. M. Ruthven, *Can. J. Chem. Eng.*, **49**, 66 (1971), b) Y. Yasuda and S. Shinbo, *Bull. Chem. Soc. Jpn.*, **61**, 745 (1988).

10) a) Y. Yasuda and G. Sugasawa, *J. Catal.*, **88**, 530 (1984), b) Y. Yasuda and A. Yamamoto, *J. Catal.*, **93**, 176 (1985).

11) Y. Yasuda, Y. Yamada, and I. Matsuura, "Proceeding of the 7th International Zeolite Conference," ed by Y. Murakami, A. Iijima, and J. W. Ward, Kodansha-Elsevier, Tokyo (1986), p. 587.

12) D. M. Ruthven, "Principles of Adsorption and Adsorption Processes," John Wiley & Sons, New York (1984), p. 124.

13) I. Suzuki, S. Oki, and S. Namba, *J. Catal.*, **100**, 219 (1986).